Cracked Carbon Matrix Decorated with Amorphous IrO_x Boosting Oxygen Evolution Reaction in Electrochemical Water Splitting

T. B. Ngoc Huynh,[a] Dohyeon Lee,[a] Soo-Kil Kim[b], Myung Jun Kim,[c,*] and Oh Joong Kwon[a,*]

[a]*Department of Energy and Chemical Engineering and Innovation Centre for Chemical Engineering, Incheon National University, Incheon 22012, Republic of Korea*

[b]*School of Integrative Engineering, Chung-Ang University, 84 Heukseok-ro, Dongjak-gu, Seoul 06974, Republic of Korea*

[c]*Department of Applied Chemistry, Kyung Hee University, Yongin-si, Gyeonggi-do 17104, Republic of Korea*

Corresponding Authors

*myungjun.kim@khu.ac.kr (M.J.K), ojkwon@inu.ac.kr (O.J.K)

Table of Contents

Supplementary Figures

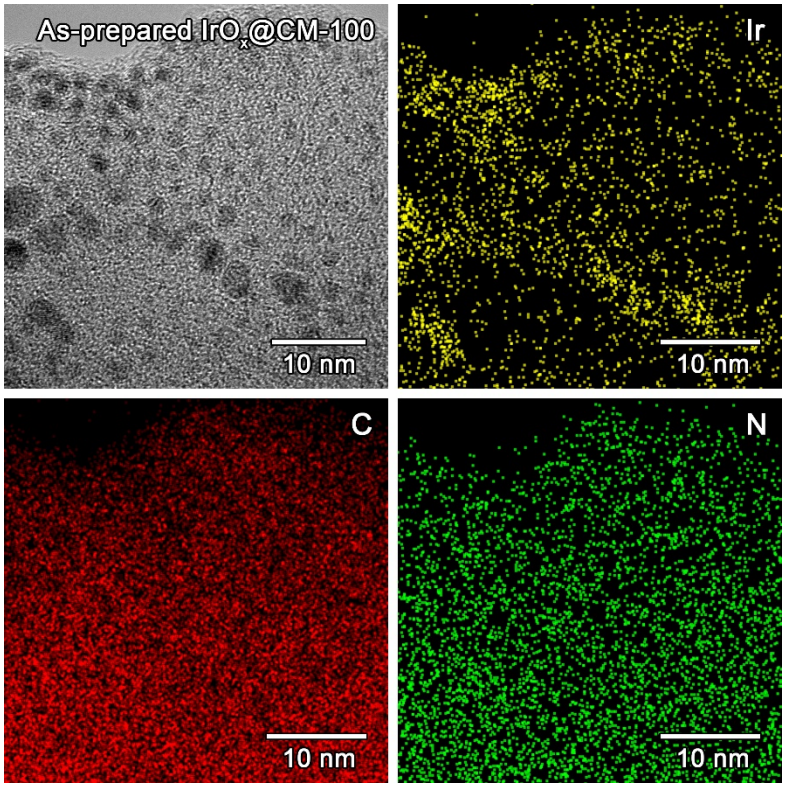

Figure S1. A TEM image and elemental mapping results of Ir nanoparticle embedded in CM-100.

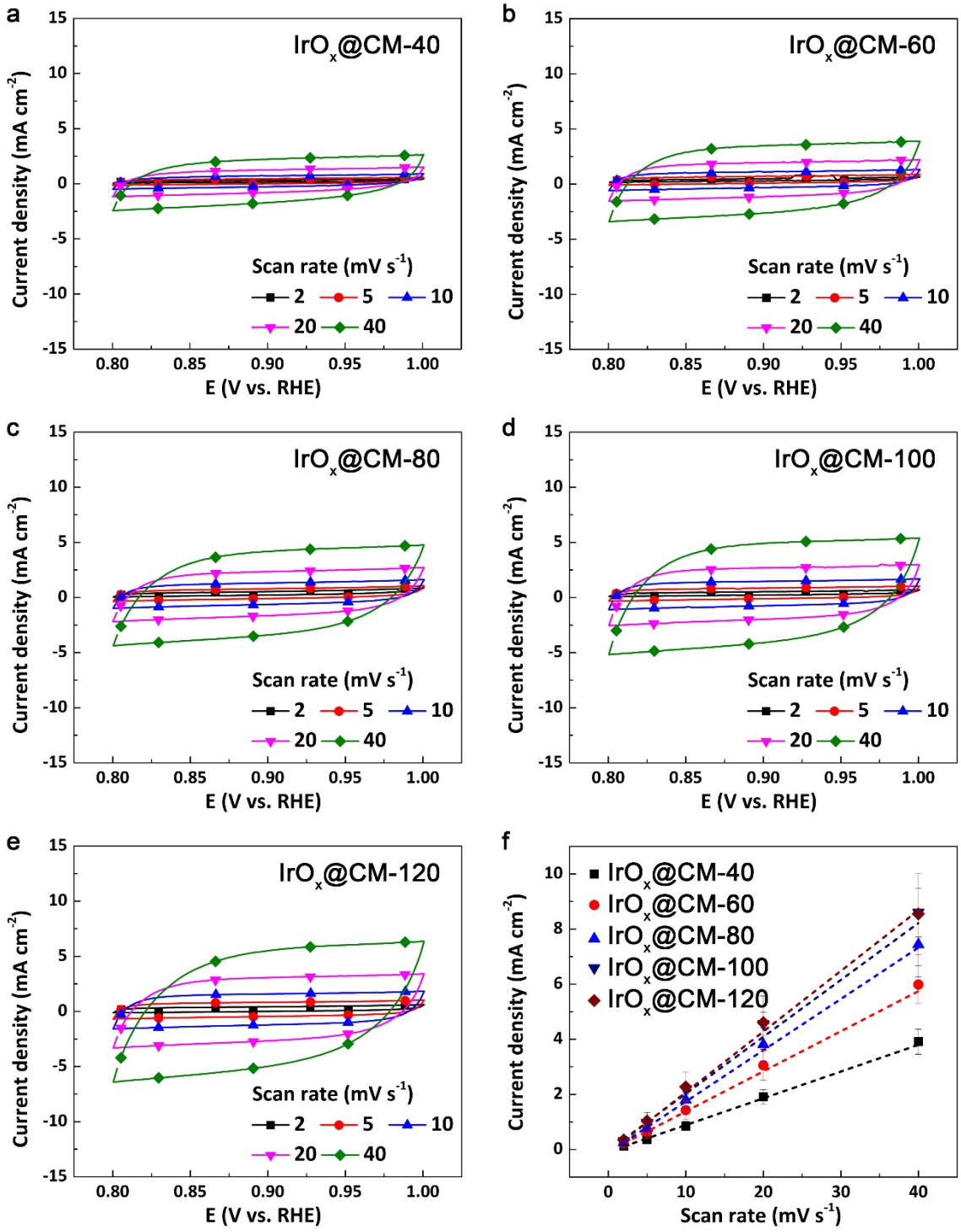

Figure S2. Cyclic voltammograms for (a) IrO_x@CM-40, (b) 60, (c) 80, (d) 100, and (e) 120 for measuring ECSA. (f) Current density as a function of the scan rate measured from (a)–(e).

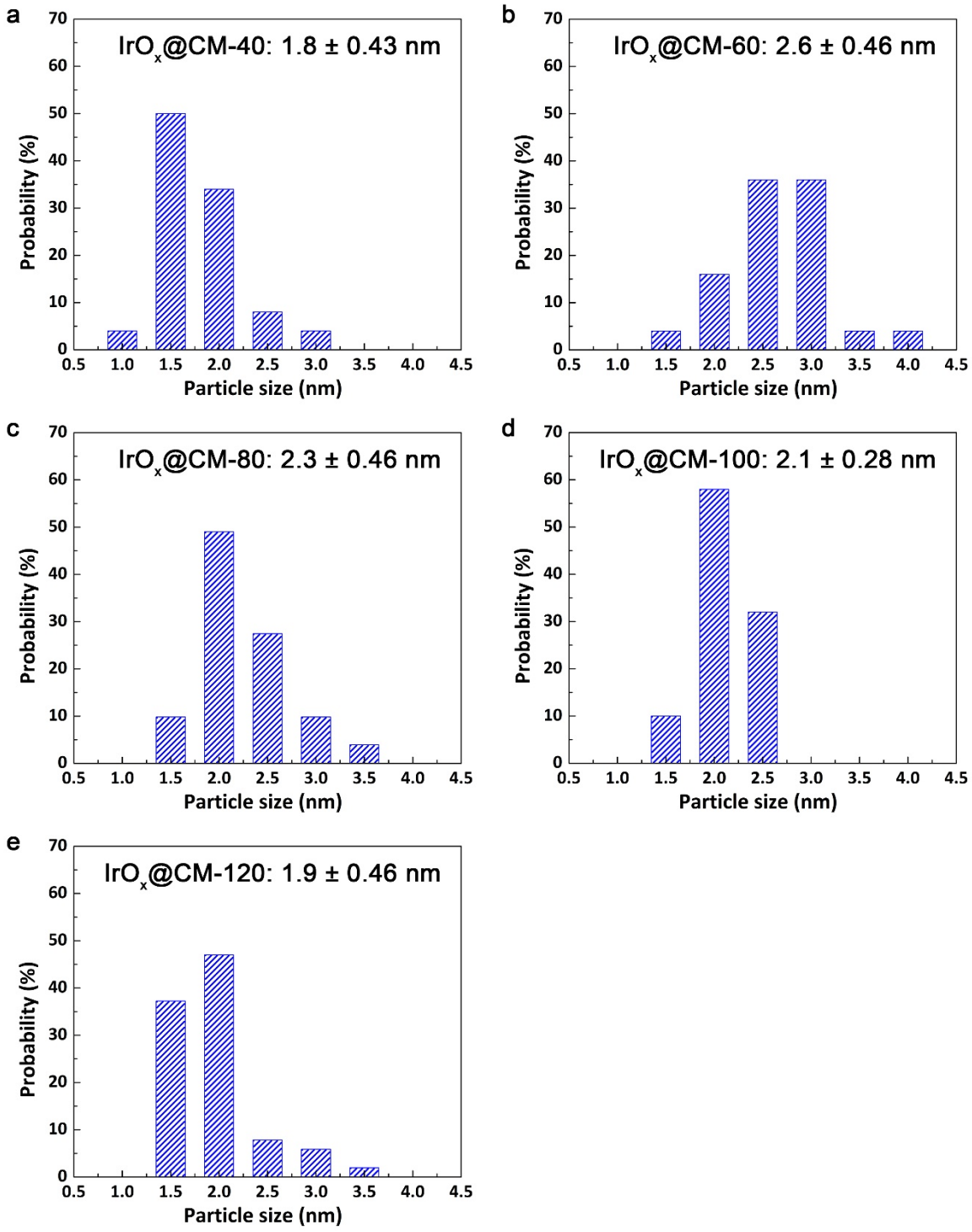

Figure S3. Size distribution of IrO_x nanoparticles embedded in (a) CM-40, (b) 60, (c) 80, (d) 100, and (e) 120.

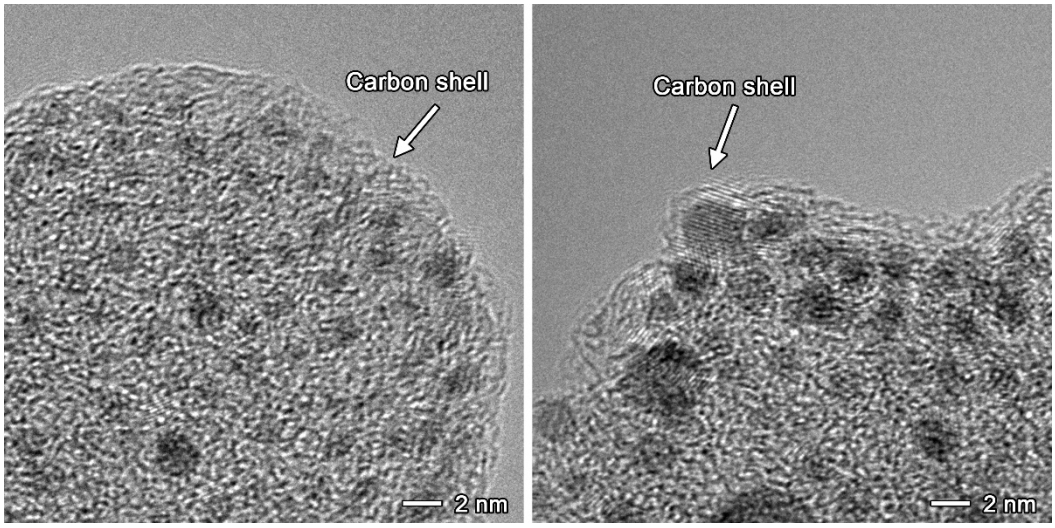

Figure S4. TEM images for IrO_x@CM-100 with white arrows indicating thin carbon layers on IrO_x particles.

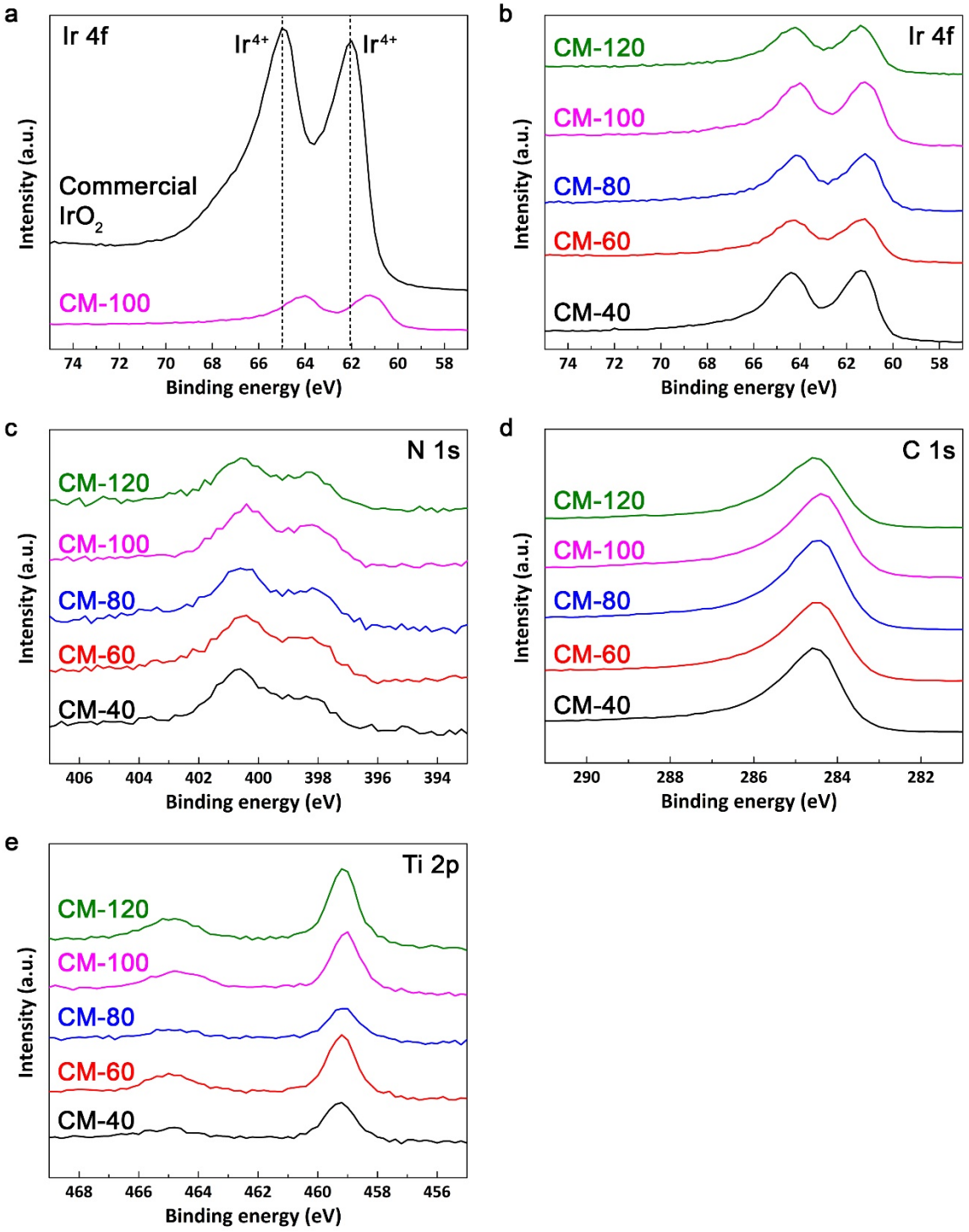

Figure S5. (a) XPS spectra of Ir 4f for commercial IrO_2 and synthesized IrO_x nanoparticles with IrO_x@CM-100. XPS spectra of (b) Ir 4f, (c) N 1s, (d) C 1s, and (e) Ti 2p for IrO_x@CM-40, 60, 80, 100, and 120.

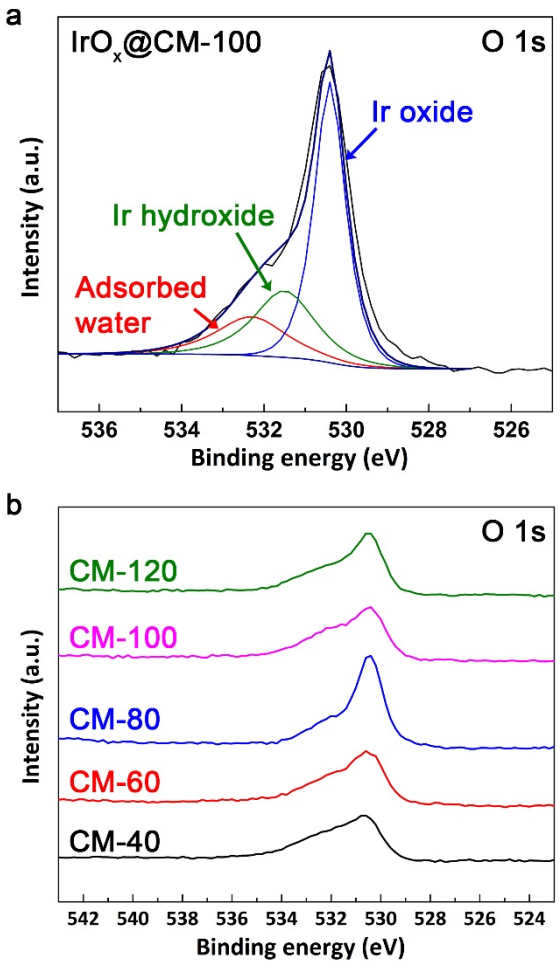

Figure S6. XPS spectra of O 1s for (a) IrO_x@CM-100 and (b) IrO_x@CM samples.

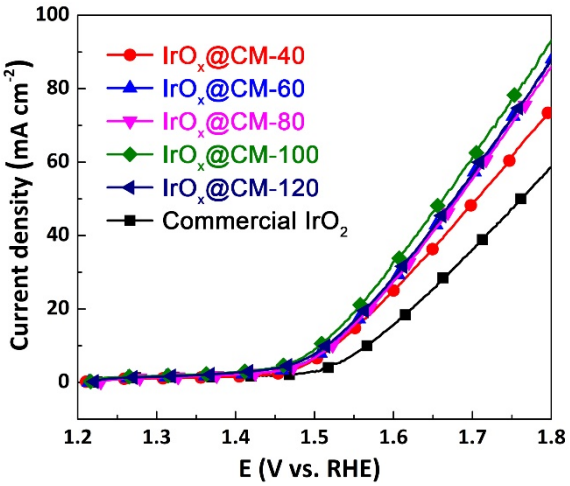

Figure S7. Voltammograms before IR correction for OER on commercial IrO_2 and IrO_x@CM samples.

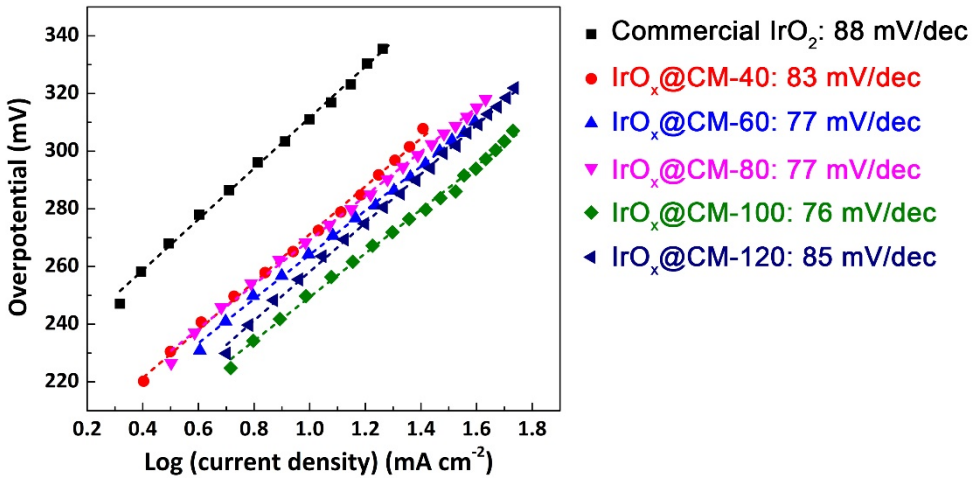

Figure S8. Tafel plots for commercial IrO_2 and IrO_x@CM samples.

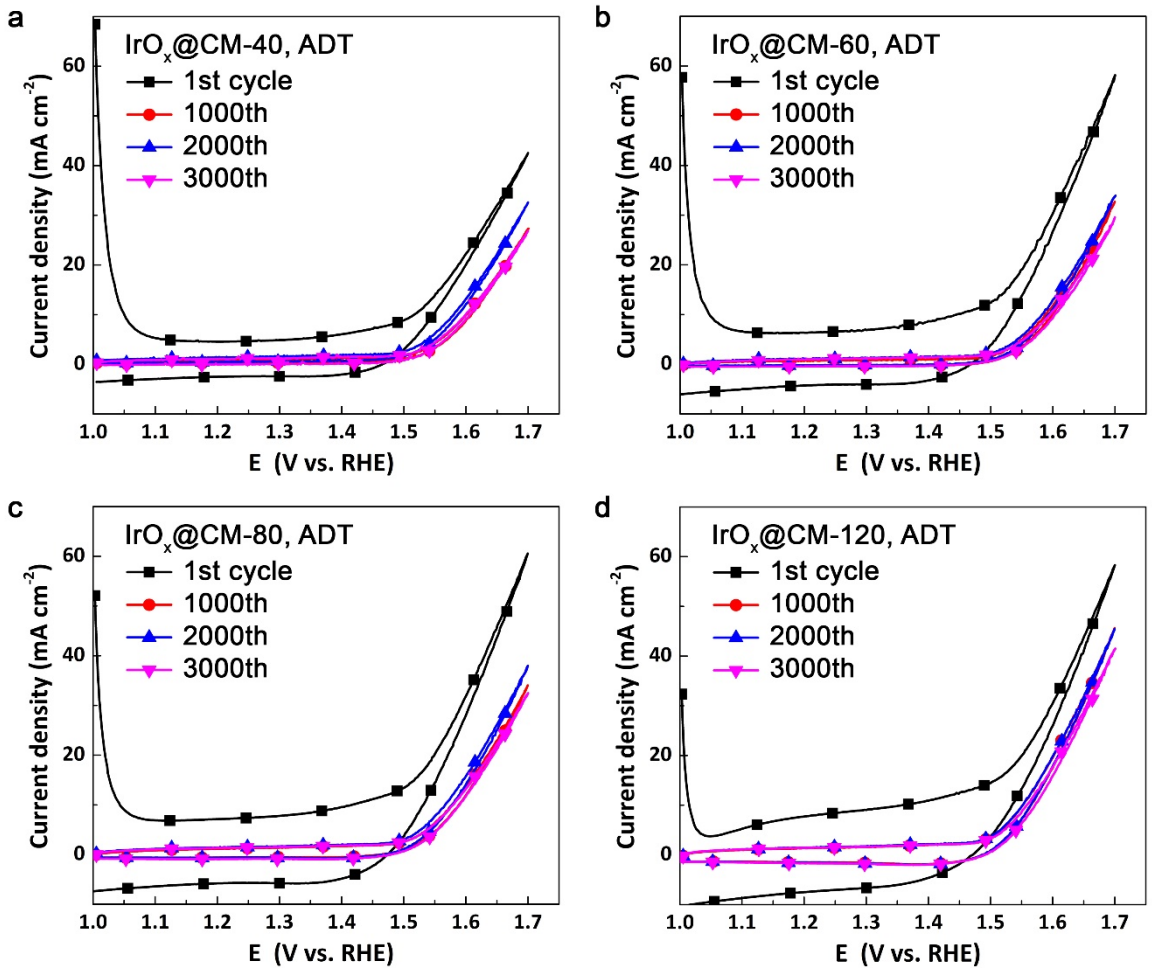

Figure S9. Voltammograms during the accelerated durability test (ADT) for (a) IrO_x@CM-40, (b) 60, (c) 80, and (d) 120 in N_2-saturated 0.1 M $HClO_4$ electrolyte.

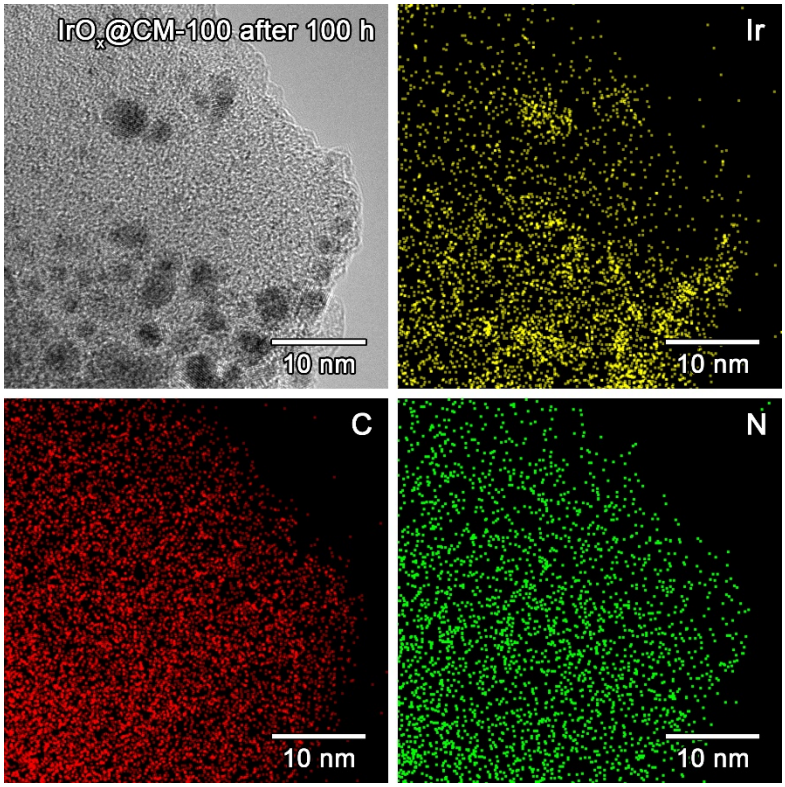

Figure S10. A TEM image and elemental mapping results of IrO_x@CM-100 after long-term durability test at 10 mA·cm^{-2} for 100 h.

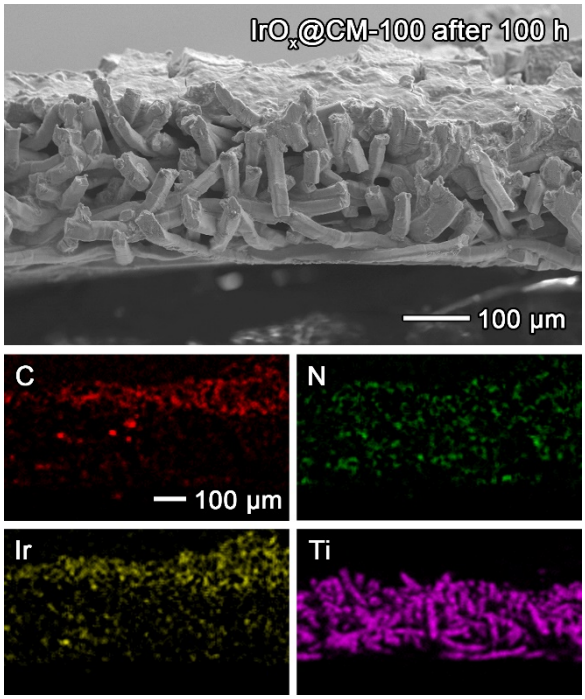

Figure S11. A SEM image and elemental mapping results of IrO_x@CM-100 after long-term durability test at 10 mA·cm^{-2} for 100 h.

Supplementary Tables

Table S1. The Synthetic Conditions for N-Doped Carbon Matrix with IrO_x Nanoparticles.

Samples	The amount of polyaniline solution[a] ($\mu L \cdot cm^{-2}$)
IrO_x@CM-40	40
IrO_x@CM-60	60
IrO_x@CM-80	80
IrO_x@CM-100	100
IrO_x@CM-120	120

[a]Polyaniline solution: 0.06 M aniline, 0.12 M F-aniline, 1 M HCl, 0.23 M $(NH_4)_2S_2O_8$ (See Experimental section)

Table S2. OER Half-Cell Performance of Ir-Based Electrocatalysts Reported in Previous Research.

Catalysts	Electrolytes	Loading Amount ($mg_{Ir}·cm^{-2}$)	η[a]	Stability test		Ref.
				Chronopoten-tiometry	Increasing rate of η	
IrO_x@CM-100	**0.1 M $HClO_4$**	**0.5**	**264**	**10 $mA·cm^{-2}$, 100 h**	**0.57 $mV·h^{-1}$**	**This study**
IrO_2-Ta_2O_5/Ti felts	0.1 M H_2SO_4	0.7	270	-	-	1
10% F-doped IrO_2/Ti foil	0.1 N H_2SO_4	0.3	250	-	-	2
2% IrO_2/NWCNT	0.5 M H_2SO_4	0.016	272	10 $mA·cm^{-2}$, 12 h	3.6 $mV·h^{-1}$	3
4wt % IrO_2/CNT	0.1 M H_2SO_4	0.076	270	10 $mA·cm^{-2}$, 12 h	3.8 $mV·h^{-1}$	4
IrW/C	0.1 M $HClO_4$	0.03	300[b]	-	-	5
Ir superstructure/ VC	0.1 M $HClO_4$	0.0115	276	10 $mA·cm^{-2}$, 5 h	7.8 $mV·h^{-1}$	6
IrNiCu /CB	0.1 M $HClO_4$	0.02	303	-	-	7
IrO_2 nanofiber	0.1 M H_2SO_4	0.2	440	-	-	8
IrO_2-RuO_2@Ru	0.5 M H_2SO_4	0.379	281	-	-	9
IrO_x nanosheets	0.5 M H_2SO_4	0.0078	250	10 $mA·cm^{-2}$, 10 h	4.7 $mV·h^{-1}$	10
3-DOM IrO2	0.5 M H_2SO_4	0.127	330	-	-	11
IrO_2/CNT	0.5 M H_2SO_4	0.016	293	10 $mA·cm^{-2}$, 10 h	5.7 $mV·h^{-1}$	12
Ir nanoparticles /graphene	0.5 M H_2SO_4	0.82	290	10 $mA·cm^{-2}$, 10 h	5.0 $mV·h^{-1}$	13
Mesoporous IrO_2 film	0.1 M $HClO_4$	-	270	-	-	14
IrO_2/graphitic carbon nitride	0.5 M H_2SO_4	0.081	276	20 $mA·cm^{-2}$, 4 h	3.4 $mV·h^{-1}$	15
$Ir_{70}Ni_{15}Co_{15}$	0.1 M $HClO_4$	0.25	220	10 $mA·cm^{-2}$, 24 h	1.4 $mV·h^{-1}$	16

[a]Overpotential@10 $mA·cm^{-2}$ (mV)

Table S3. Charge Transfer and Solution Resistances Measured from Nyquist Plots in Figure 4(c).

Samples	Solution resistance (R_s, Ω·cm^2)	Film resistance (R_f, Ω·cm^2)	Charge transfer resistance (R_{ct}, Ω·cm^2)
IrO_x@CM-40	2.90	1.38	5.35
IrO_x@CM-60	2.60	1.30	3.24
IrO_x@CM-80	2.64	1.03	3.76
IrO_x@CM-100	2.60	0.17	3.20
IrO_x@CM-120	2.56	0.84	3.90
Commercial IrO_2	2.53	2.02	10.82

Table S4. Percentages of Oxygen Species Calculated from XPS Spectra in Figure S6(b).

Samples	Lattice O	OH group
IrO_x@CM-40	49.5	50.5
IrO_x@CM-60	54.1	45.9
IrO_x@CM-80	52.5	47.5
IrO_x@CM-100	46.2	53.8
IrO_x@CM-120	54.0	46.0

Table S5. Full-Cell Performance of Ir-Based Electrocatalysts Reported in Previous Research.

Catalysts		Membrane	T cell (°C)	Cell voltage @1A·cm^{-2} (V)	Ref.
Anode	**Cathode**				
IrO_x@CM-100 (1 mg·cm^{-2})	**Pt/C 40% (0.4 mg·cm^{-2})**	**NR115**	**90**	**1.64**	**This study**
Ir/TiO_2-MoOx (0.5 mg·cm^{-2})	Pt/C 46% (0.5 mg·cm^{-2})	NR212	80	1.74	17
Ir/B4C-100 °C (0.5 mg·cm^{-2})	Pt/C 20% (0.4 mg·cm^{-2})	NR212	80	1.63	18
$Ir_{0.7}Ru_{0.3}O_x$ (1.8 mg·cm^{-2})	Pt/C (0.5 mg·cm^{-2})	NR115	80	1.656	19
IrO_2 (1.4 mg·cm^{-2})	Pt/C 40% (0.4 mg·cm^{-2})	NR115	80	1.765	20
IrO_2 (3.0 mg·cm^{-2})	Pt/C (0.1 mg·cm^{-2})	NR212	RT	1.56	21
$Ir_{0.52}Sn_{0.48}O_2$ (1.5 mg·cm^{-2})	Pt/C 70% (0.57 mg·cm^{-2})	NR115	80	1.63	22
IrO_2@TiO_2 (1.2 mg·cm^{-2})	Pt/C 60% (0.5 mg·cm^{-2})	NR115	80	1.7	23
IrO_2-V doped TiO_2 (2.5 mg·cm^{-2})	Pt/C 40% (0.5 mg·cm^{-2})	NR117	80	2.03	24
IrO_2-Nb doped TiO_2 (2.5 mg·cm^{-2})	Pt/C 40% (0.5 mg·cm^{-2})	NR117	80	2.027	25
IrO_2 (1.7 mg·cm^{-2})	Pt/C 40% (0.5 mg·cm^{-2})	NR117	80	1.88	26
80% IrO_2/ATO (2 mg·cm^{-2})	Pt/C 20% (0.5 mg·cm^{-2})	NR115	80	1.74	27

References

1 F. Amano, Y. Furusho and Y. M. Hwang, *ACS Appl. Energy Mater.*, 2020, **3**, 4531–4538.

2 K. S. Kadakia, P. H. Jampani, O. I. Velikokhatnyi, M. K. Datta, S. K. Park, D. H. Hong, S. J. Chung and P. N. Kumta, *J. Power Sources*, 2014, **269**, 855–865.

3 X. Wen, L. Bai, M. Li and J. Guan, *Mater. Today Energy*, 2018, **10**, 153–160.

4 R. Badam, M. Hara, H. H. Huang and M. Yoshimura, *Int. J. Hydrogen Energy*, 2018, **43**, 18095–18104.

5 F. Lv, J. Feng, K. Wang, Z. Dou, W. Zhang, J. Zhou, C. Yang, M. Luo, Y. Yang, Y. Li, P. Gao and S. Guo, *ACS Cent. Sci.*, 2018, **4**, 1244–1252.

6 Y. Pi, N. Zhang, S. Guo, J. Guo and X. Huang, *Nano Lett.*, 2016, **16**, 4424–4430.

7 J. Park, Y. J. Sa, H. Baik, T. Kwon, S. H. Joo and K. Lee, *ACS Nano*, 2017, **11**, 5500–5509.

8 F. Hegge, F. Lombeck, E. Cruz Ortiz, L. Bohn, M. Von Holst, M. Kroschel, J. Hübner, M. Breitwieser, P. Strasser and S. Vierrath, *ACS Appl. Energy Mater.*, 2020, **3**, 8276–8284.

9 G. Li, S. Li, J. Ge, C. Liu and W. Xing, *J. Mater. Chem. A*, 2017, **5**, 17221–17229.

10 B. Jiang, J. Kim, Y. Guo, K. C. W. Wu, S. M. Alshehri, T. Ahamad, N. Alhokbany, J. Henzie and Y. Yamachi, *Catal. Sci. Technol.*, 2019, **9**, 3697–3702.

11 W. Hu, Y. Wang, X. Hu, Y. Zhou and S. Chen, *J. Mater. Chem. View*, 2012, **22**, 6010.

12 J. Guan, D. Li, R. Si, S. Miao, F. Zhang and C. Li, *ACS Catal.*, 2017, **7**, 5983–5986.

13 J. Zhang, G. Wang, Z. Liao, P. Zhang, F. Wang, X. Zhuang, E. Zschech and X. Feng, *Nano Energy*, 2017, **40**, 27–33.

14 E. Ortel, T. Reier, P. Strasser and R. Kraehnert, *Chem. Mater.*, 2011, **23**, 3201–3209.

15 J. Chen, P. Cui, G. Zhao, K. Rui, M. Lao, Y. Chen, X. Zheng, Y. Jiang, H. Pan, S. X. Dou and W. Sun, *Angew. Chemie - Int. Ed.*, 2019, **58**, 12540–12544.

16 Y. Zhao, M. Luo, S. Chu, M. Peng, B. Liu, Q. Wu, P. Liu, F. M. F. de Groot and Y. Tan, *Nano Energy*, 2019, **59**, 146–153.

17 E. J. Kim, J. Shin, J. Bak, S. J. Lee, K. hyun Kim, D. H. Song, J. H. Roh, Y. Lee, H. W. Kim, K. S. Lee and E. A. Cho, *Appl. Catal. B Environ.*, 2021, **280**, 119433.

18 J. Islam, S. K. Kim, P. T. Thien, M. J. Kim, H. S. Cho, W. C. Cho, C. H. Kim, C. Lee and J. H. Lee, *J. Power Sources*, 2021, **512**, 230506.

19 M. Faustini, M. Giraud, D. Jones, J. Rozière, M. Dupont, T. R. Porter, S. Nowak, M. Bahri, O. Ersen, C. Sanchez, C. Boissière, C. Tard and J. Peron, *Adv. Energy Mater.*, 2019, **9**, 1–11.

20 S. Choi, S. H. Shin, D. H. Lee, G. Doo, D. W. Lee, J. Hyun, J. Y. Lee and H. T. Kim, *J. Mater. Chem. A*, 2022, **10**, 789–798.

21 H. Su, B. J. Bladergroen, V. Linkov, S. Pasupathi and S. Ji, *Int. J. Hydrogen Energy*, 2011, **36**, 15081–15088.

22 G. Li, H. Yu, X. Wang, S. Sun, Y. Li, Z. Shao and B. Yi, *Phys. Chem. Chem. Phys.*, 2013, **15**, 2858–2866.

23 C. Van Pham, M. Bühler, J. Knöppel, M. Bierling, D. Seeberger, D. Escalera-López, K. J. J. Mayrhofer, S. Cherevko and S. Thiele, *Appl. Catal. B Environ.*, 2020, **269**, 118762.

24 C. Hao, H. Lv, Q. Zhao, B. Li, C. Zhang, C. Mi, Y. Song and J. Ma, *Int. J. Hydrogen Energy*, 2017, **42**, 9384–9395.

25 C. Hao, H. Lv, C. Mi, Y. Song and J. Ma, , DOI:10.1021/acssuschemeng.5b00531.

26 H. J. Ban, M. Y. Kim, D. Kim, J. Lim, T. W. Kim, C. Jeong, Y. A. Kim and H. S. Kim, *J. Electrochem. Sci. Technol.*, 2019, **10**, 22–28.

27 V. K. Puthiyapura, M. Mamlouk, S. Pasupathi, B. G. Pollet and K. Scott, *J. Power Sources*, 2014, **269**, 451–460.